IEEE Access
Multidisciplinary | Rapid Review | Open Access Journal

Received May 14, 2019, accepted June 10, 2019, date of publication June 20, 2019, date of current version July 10, 2019.

Digital Object Identifier 10.1109/ACCESS.2019.2924197

CMIP5-Based Wave Energy Projection: Case Studies of the South China Sea and the East China Sea

CHONG-WEI ZHENG[1,2,3,4], GUO-XIANG WU[5], XUAN CHEN[6], QING WANG[1], ZHAN-SHENG GAO[4], YUN-GE CHEN[4], AND XIA LI[7]

[1]Coast Institute, Ludong University, Yantai 264025, China
[2]State Key Laboratory of Numerical Modeling for Atmospheric Sciences and Geophysical Fluid Dynamics (LASG), Institute of Atmospheric Physics, Chinese Academy of Sciences, Beijing 100029, China
[3]State Key Laboratory of Estuarine and Coastal Research, Shanghai 200062, China
[4]Dalian Naval Academy, Dalian 116018, China
[5]College of Engineering, Ocean University of China, Qingdao 266100, China
[6]The 75839 Army of the PLA, Guangzhou 510510, China
[7]College of Meteorology and Oceanography, National University of Defense Technology, Nanjing 211101, China

Corresponding authors: Qing Wang (schingwang@126.com) and Chong-Wei Zheng (chinaoceanzcw@sina.cn)

This work was supported in part by the Open Research Fund of State Key Laboratory of Estuarine and Coastal Research under Grant SKLEC-KF201707, in part by the National Science Foundation of China–Shandong United Fund under Grant U1706220, in part by the National Natural Science Foundation of China under Grant 41490642 and Grant 51709243, and in part by the Natural Science Foundation of Shandong Province, China, under Grant ZR2019BD005.

ABSTRACT Wave energy development will help ease resource crises. The projection of wave energy has practical value for the long-term planning of energy development (implementation of power generation, trading strategies, and so on). This paper proposed a wave energy projection program. South China Sea (SCS) and the East China Sea (ECS) in 2019 were carried out as case studies using the Coupled Model Intercomparison Project Phase 5 (CMIP5) dataset to drive the WAVEWATCH-III (WW3) wave model. The multiyear average wave energy of the SCS and ECS was presented. A comparison of the projected values with multiyear averages of the wave energy could positively contribute to the planning of the wave energy development. The results show that the SCS possessed relatively rich energy for both the past and future and that January and October possessed the highest wave power density (WPD). The projected annual average WPD in 2019 was similar to the multiyear average WPD in the north and middle of the ECS, slightly higher than the multiyear average in the south of the ECS, and considerably greater than that in the SCS. The projected WPDs in January, April, and October 2019 were higher than the multiyear averages in the corresponding months. In July, the projected WPD in the SCS was smaller than the multiyear average, while the opposite was observed in the south of the ECS. The projected effective wave height occurrence (EWHO) and the occurrence of WPD >2 kW/m in 2019 were also superior to the multiyear average values.

INDEX TERMS East China Sea, South China Sea, WAVEWATCH-III, wave energy resource, projection program, multiyear average status.

I. INTRODUCTION

Clean, unpolluted, and renewable wave energy is a good solution to environmental and resource crises [1]–[4]. For the optimal development of energy, its characteristics must be evaluated [5]–[10]. Wave energy evaluation includes the following stages with respect to the data: the observation stage, the hindcast stage, and the reanalysis stage. By using limited data from marine ships and wave buoys, Hulls [11] and Denis [12] provided an overview of the global coastal WPD distribution. They reported that the concentrated wave energy zones in the world are in the northeastern part of the North Atlantic and along the Pacific coast of North America, the southern coast of Australia, the Chilean coast in South America, and the southwestern coast of South Africa. Along with the rapid development of marine remote-sensing

The associate editor coordinating the review of this manuscript and approving it for publication was Eklas Hossain.

and numerical simulation technology, increasing amounts of satellite altimeter wave data and hindcast wave data have been used to analyze wave energy resources. Cornett [13] simulated the global wave field for the period from 1997–2006 by using the WW3 wave model and then calculated the distribution and variation in the global WPD. He stated that the amount of available wave power, the steadiness of this supply, and the frequency and intensity of extreme wave conditions are critical factors influencing the site selection of wave energy projects. Aydogan *et al.* [14] evaluated the wave energy of the Black Sea by using 13-year hindcast wave data forced with wind data from the European Centre for Medium-Range Weather Forecasts (ECMWF). Their results revealed that the wave energy decreases along the coast from west to east. The most energetic region in terms of the WPD is the southwestern part of the Black Sea, whereas the eastern part of the Black Sea is the least energetic. Zheng and Li [15] proposed a wave energy classification scheme that comprehensively incorporates energy factors, environmental risk factors and cost factors. The results can provide a scientific reference for wave power plant locations. Sierra *et al.* [16] analyzed the impact of climate change on wave energy resources, and Menorca was selected as a case study. The result showed slight general decreases in the annual and seasonal wave powers (except for in the summer).

Previous studies made notable contributions to wave energy assessments, including presenting the recent progress in determining the temporal-spatial distribution of wave energy parameters and the energy classification. However, few studies have considered the projection of wave energy, which has practical value for the long-term planning of wave energy development. A comparison between the projected values and multiyear average values of the wave energy could positively contribute to the long-term planning of wave energy development (implementation of power generation, trading strategies, etc.). Just as comparing the temperature of a winter with the Multiyear average winter temperature can determine whether it is a warm winter or a cold winter, a comparison of the energy of a year with the Multiyear average energy can determine whether it is an energy-rich year or an energy-poor year. The projection results can be used to determine whether the output of wave energy resources meets the demand or whether there is an energy gap and the required supplementation from other energy sources can be accurately calculated. In this study, a wave energy projection program was proposed, and the ECS and SCS were selected as case studies.

II. DATA AND METHODOLOGY

A. DATA

In this study, two wind datasets, namely, the cross-calibrated multi-platform (CCMP) and the CMIP5 were employed as the driving fields of the WW3 wave model. The CCMP wind data on 0.25° × 0.25° grids at 6-hour intervals were provided by the Physical Oceanography Distributed Active Archive Center (PO.DAAC) [17]. The time range is from July 1987 to December 2011, and the spatial range is from 78.375°S–78.375°N to 0.125°–359.875°E. The CMIP5 wind data used in this study are the representative concentration pathway (RCP) 4.5 scenario data from the National Oceanic and Atmospheric Administration (NOAA) Geophysical Fluid Dynamics Laboratory (GFDL), which are widely used in climate change analysis, wind energy evaluation, etc. [18]. The RCP4.5 was chosen because it is an intermediate ''stable without overshoot'' pathway [19]–[21]. RCP4.5 is a scenario that stabilizes the radiative forcing at 4.5 W/m^2 in the year 2100 without ever exceeding that value. RCP4.5 includes long-term global emissions of greenhouse gases, short-lived species, and land-use-land-cover data in a global economic framework. The time resolution of the CMIP5 is 3 hours, the spatial resolution is 2.5° × 2.0°, the time range is from January 2006 to December 2099, and the spatial range is from 89°S–89°N to 1.25°–358.75°E. The CMIP5 data is widely used in the analysis of global climate change, including research on future wave fields, extreme wave heights, etc. [18], [21], [22].

B. METHODOLOGY

This study proposed a projection system for wave energy resources. The wave energy projection of the China seas (including the ECS and the SCS) for 2019 was selected as a case study. The program includes three main parts. First, the WW3 wave model was employed to simulate the future wave data driven by the CMIP5 wind dataset. Second, using the WW3 wave model with the CCMP wind data as a driving field, a long-term series of climatic wave data was obtained. Third, based on the collected and projected climatic wave data, the future and past wave energy were compared to provide a reference for the long-term planning of wave energy development. Referring to this method, the wave energy under different scenarios (RCP2.6, RCP6.0, and RCP8.5) for longer time series and over a wider range can also be projected in future work.

Previous studies have made great contributions to the simulation analysis of the wave climate of the China seas [23]–[26]. Their results demonstrated the good simulation ability of the third-generation wave models of the WW3 and Simulated Waves Nearshore (SWAN) for the wave fields of the China seas. Thus, the WW3 wave model is suitable and has high credibility for China seas. Previous studies have also shown that it is feasible to use the CMIP5 data-driven wave model to obtain and analyze future wave data [27]–[29]. Thus, the WW3 wave model was employed to simulate the wave field of the China seas.

The detailed method of wave energy projection is as follows.

First, the 3-hourly wave field of the China seas for the period from 00:00 January 1, 2019, to 18:00 December 31, 2019, was simulated using the WW3 wave model driven by the CMIP5 wind data (shortened as wave data-CMIP5). To improve the simulation precision, the region of interest

was extended and nested (as shown in Figure 1). The expansion region is 5°S ∼ 45°N, 90°E ∼ 180°E, and the calculation spatial resolution for the extended region is 0.5° × 0.5°. The focus area is 0° ∼ 40°N, 100°E ∼ 135°E, and the calculation spatial resolution of the focus area is 0.25° × 0.25°. The calculation time step is 900 seconds, and the simulated wave field data are recorded every 3 hours. The simulated wave data from the extended area provide the boundary conditions for the wave simulation of the focus area.

Second, a 3-hourly hindcast of the China seas wave data for the period from January 1, 1988, to December 31, 2011, (denoted wave data-CCMP) was obtained using the WW3 wave model driven by the CCMP wind data. A comparison of the wave data-CCMP with the observed buoy data from Japan's "SATA Cape" and "Fukue Island" and Korea's "Cheju Island" and Korea station 22001 indicated that the hindcasted wave data were reliable [30].

Third, the Multiyear average wave energy in the China seas was retrieved from the wave data-CCMP, where the wave energy in 2019 was projected using the wave data-CMIP5. Then, the projected values and multiyear average values of the wave energy parameters (including the WPD, EWHO and WPD levels) were compared to provide a reference for the long-term planning of wave energy development.

III. RESULTS AND DISCUSSION

A. WPD CALCULATION METHOD

This study utilized the WPD calculation method given by Iglesias and Carballo [31], Vosough [32] and Wan *et al.* [33], [34] to collect the 3-hourly WPD in the ECS and SCS for the period from January 1988 to December 2011 (shortened as WPD-CCMP) from the 3-hourly wave data-CCMP. Using the same method, the 3-hourly WPD for the period from January to December 2019 (shortened as WPD-CMIP5) was also obtained from the 3-hourly wave data-CMIP5.

In shallow water ($d/\lambda < 1/20$), the calculation method is as follows:

$$P_w = \frac{\rho g}{16} H_s^2 \sqrt{gd} \tag{1}$$

In deep water ($d/\lambda \geq 1/2$), the calculation method is as follows:

$$P_w = \frac{\rho g^2}{64\pi} H_s^2 T_e = 0.49 H_s^2 T_e \tag{2}$$

In medium water ($1/20 \leq d/\lambda < 1/2$), the calculation method is as follows:

$$P_w = \bar{E}\left(\frac{gT_e}{2\pi}\tanh kd\right)\left[\frac{1}{2}\left(1 + \frac{2kd}{\sinh 2kd}\right)\right] \tag{3}$$

Here, P_w is the WPD (kW/m), H_s is the significant wave height (SWH) (m), T_e is the energy period (s), ρ is the sea water mass density (∼1 028 kg/m^3), g is the gravitational acceleration (9.8 m/s^2), π is the ratio of the circumference to the diameter (3.14), d is the water depth (m), and λ is the wave length (m).

B. SPATIAL DISTRIBUTION OF WPD

By averaging the values of the WPD-CCMP at each grid point from 1988 to 2011, the 24-year average WPD in the ECS and SCS was obtained (Figure 2a). Using the same method, the annual average WPD in 2019 in the ECS and SCS could also be determined (Figure 2b).

1) MULTIYEAR AVERAGE WPD

The area with WPD > 18 kW/m was mainly distributed in the north of the SCS with a large center located in the Luzon Strait and its west adjacent waters. Indigent areas with WPD < 3 kW/m were located in the north and mid-north of the ECS, the coast of the middle of the ECS, the Beibu Gulf, the Gulf of Thailand, and the equatorial waters. The south of the ECS and most of the SCS were relatively WPD-rich regions. The WPD was >6 kW/m in most of the south of the ECS and 12–15 kW/m in the waters of the Ryukyu Islands. The WPD was >9 kW/m north of 10°N in the SCS.

2) PROJECTED WPD

In 2019, the projected WPD was similar to the multiyear average WPD in the north and middle of the ECS and was slightly larger than the multiyear average WPD in the south of the ECS. In the south of the ECS, the area with WPD >15 kW/m had values that were obviously larger than the multiyear average. In the SCS, the WPD was notably larger than the multiyear average. The WPD in a large portion of the middle of the SCS was >15 kW/m, which is clearly greater than the multiyear average (>9 kW/m). There is also a significant increase in the eastern waters of the Philippines, with a large area having a WPD of >21 kW/m, which is obviously greater than the multiyear mean (>9 kW/m). Wang *et al.* [21] projected the global wave height. Mori *et al.* [22] presented the mean of the SWH in the present and future climates. The results of Wang *et al.* [21] and Mori *et al.* [22] found a relatively large area of high SWHs distributed in the belt of the Ryukyu Islands-Luzon Strait-traditional gale center of the SCS (southeast of the Indo-China Peninsula). Casas-Prat *et al.* [29] found agreement between the climatological mean SWH and an ensemble-projected SWH. Mori *et al.* [35], Hemer *et al.* [36], and Camus *et al.* [37] projected the future changes of the annual mean SWH, and slight decreases were found in most of the China seas. The spatial distribution exhibits overall agreement between their results and the results of this study in the China seas.

C. SEASONAL DISTRIBUTION OF WPD

The development of the wave energy is significantly impacted by the seasonal differences in the WPD. Figure 3 presents the WPD-CCMP and WPD-CMIP5 in January, April, July and October.

1) MULTIYEAR AVERAGE WPD

In January (representing the winter, as presented in the following), the WPD was the highest among the year-round

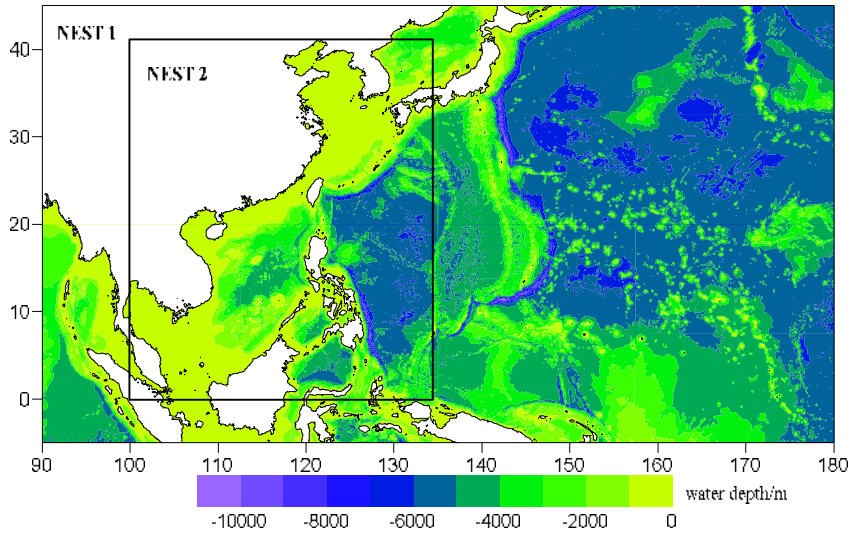

FIGURE 1. Geographic features of the East China Sea and South China Sea.

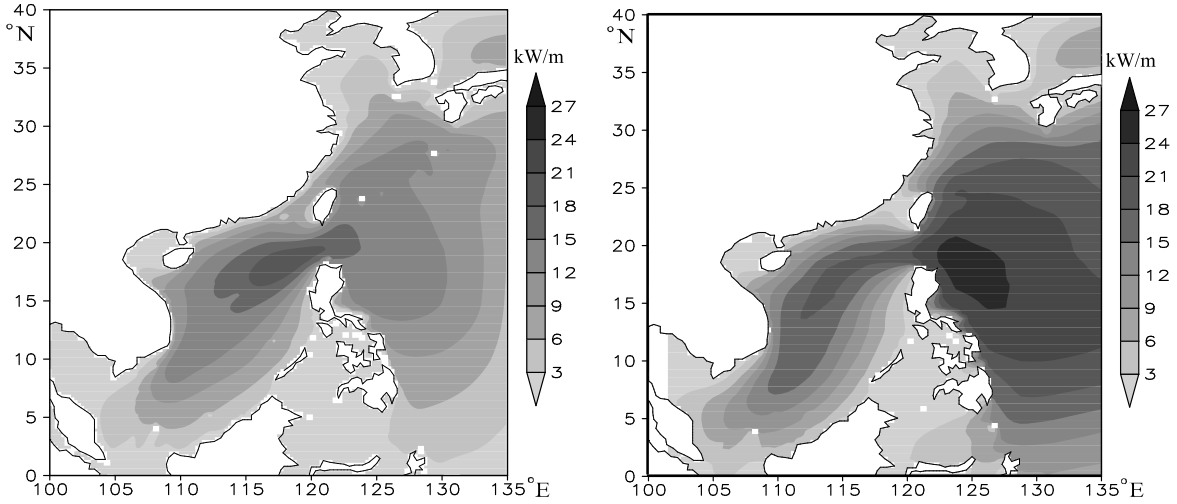

FIGURE 2. Multiyear average wave power density for the period 1988-2011 (left) and the projected wave power density in 2019 (right).

values due to the influence of frequent cold air. The WPDs in the SCS and the south of the ECS were higher than those in the other waters. Two obvious high-value centers were the Luzon Strait and its western adjacent waters (>27 kW/m) and the southeastern waters of the Indochina Peninsula (the traditional gale center of the SCS; >21 kW/m). In April (representing the spring, as presented in the following), the WPD was the lowest of the year-round values. A relatively large area with WPDs of 5–7 kW/m was located in the waters of the Ryukyu Islands. In July (representing the summer, as presented in the following), the WPD was slightly higher than that in April. A relatively large area with WPDs of 9–13 kW/m was located in the waters of the Ryukyu Islands, followed by the traditional gale center of the SCS (7–10 kW/m). In October (representing the autumn, as presented in the following), the WPD was slightly lower than that in January but considerably greater than those in April and July. The WPDs in most areas of the SCS and the south of the ECS were >6 kW/m, with a large center located in the Luzon Strait and its surrounding waters (>24 kW/m).

2) PROJECTED WPD

Overall, in January, April and October, the projected WPDs exceeded the multiyear averages in the corresponding months in most of the ECS and SCS. In January, the WPD was the highest among the year-round values and far beyond the multiyear averages in the traditional gale center of the SCS and the eastern waters of the Philippines. In April, these two counterparts were quite similar in the ECS. Note that the WPD in April was the lowest for both the multiyear average and for the 2019 projection. In July, the WPD decreased to its minimum in most parts of the ECS and SCS. The projected

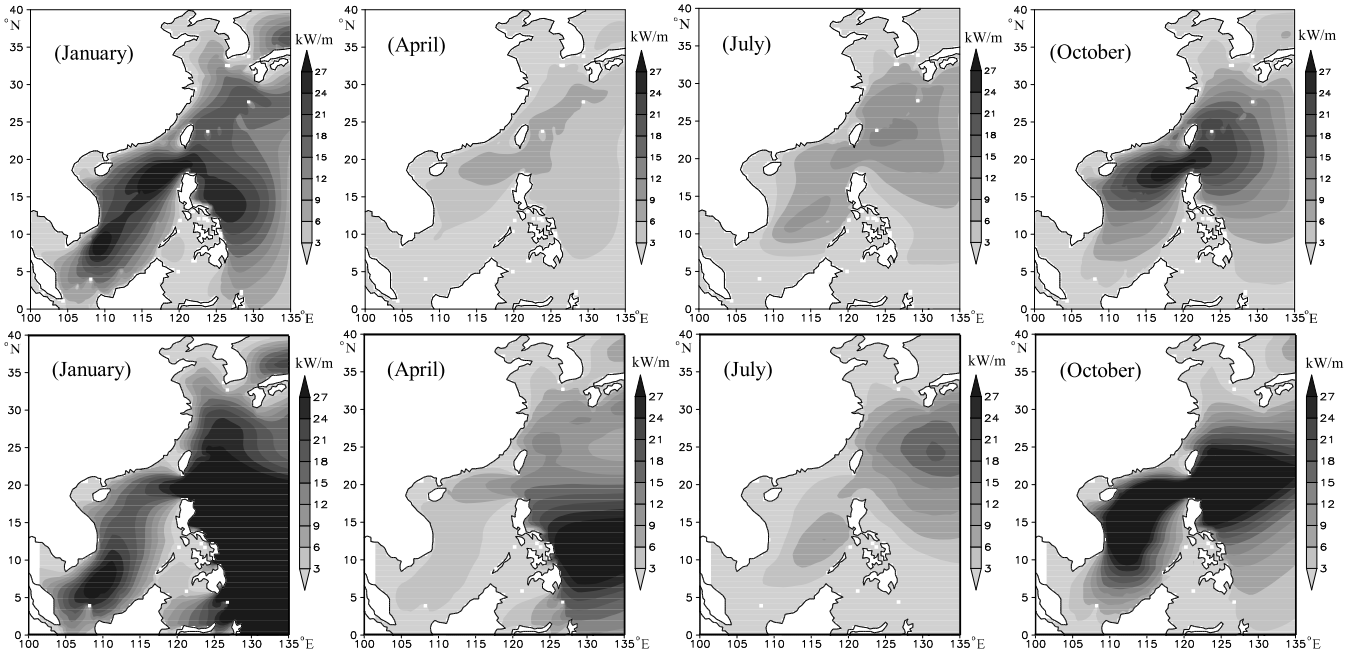

FIGURE 3. Multiyear average wave power density (up) and projected wave power density in 2019 (down).

WPD in the SCS was smaller than the multiyear averages, while the opposite trend was observed in the south of the ECS. In October, the WPD was somewhat higher: it was <6 kW/m in the north and middle of the ECS, the Beibu Gulf, the Gulf of Thailand, and the equatorial waters; >15 kW/m in the center and north of the SCS; and >24 kW/m in the Luzon Strait and its adjacent waters.

D. MONTHLY WPD VARIATION IN IMPORTANT REGIONS

The monthly characteristics of the projected WPD in 2019 are presented in Figure 4. The traditional gale center of the SCS and the Luzon Strait were selected as the case studies. The WPD was averaged from January 1st 0000UTC to 31st 2100UTC, 2019, and consequently the monthly mean WPD in each 0.25° × 0.25° grid was obtained. Then, the Thiessen polygon method was used to obtain a regional average of the WPD in the traditional gale center of the SCS. Subsequently, using the same method, the monthly values (from January to December 2019) in the traditional gale center of the SCS and the Luzon Strait were acquired (Figure 4).

As shown in Figure 4, in the traditional gale center of the SCS, the WPD in the winter was prominently larger than that in the other seasons. For instance, in January, it can reach 41 kW/m. In the Luzon Strait, the WPD in November (approximately 67 kW/m) was much greater than that in the other months. Nonetheless, during the summer, the WPDs in the above two regions were both lower. In general, the WPD in the traditional gale center of the SCS exhibited an obvious monthly variation in 2019, but this variation was not as great as that in the Luzon Strait.

E. OCCURRENCE OF EXPLOITABLE WAVES

In terms of the wave energy development, waves with an SWH > 1.3 m in the ocean are usually regarded as exploitable waves, while those with an SWH of 4.0 m or greater have a significant destructive capability. Zheng and Li [15] thus referred to a SWH between 1.3–4.0 m as the effective wave height for wave energy development. Obviously, the EWHO reflects the availability of wave energy. Among the fast-developing wave energy devices, some of them can well absorb wave energy when the SWH is >0.5 m. Therefore, the range of exploitable SWHs will continue to expand. Based on the simulated wave data for 2019 at 3-hour intervals, the EWHO in the different seasons was determined (Figure 5).

In January, the exploitable SWHs presented the highest year-round values. In most of the SCS, the occurrence was >60%. In the traditional gale center of the SCS, the Luzon Strait and the eastern waters of the Philippines, the occurrence was >90%. The occurrence was >60% in most of the south of the ECS, 30%–60% in the central and southern areas of the middle of the ECS, and poor (<10%) in the north of the ECS, the northern area of the middle of the ECS, and some near-shore waters. In April, the occurrence of exploitable SWHs was identified as the lowest (<30%) of the year-round values in most of the SCS. Most of the SCS showed values of 10%–30%, with 20%–50% in most of the south of the ECS, >90% in the eastern waters of the Philippines, and 10%–50% in the central-southern areas of the middle of the ECS. The low-value areas (<10%) were mainly distributed in the north of the ECS, the Beibu Gulf, the Gulf of Thailand, and the equatorial waters. In July, the occurrence of

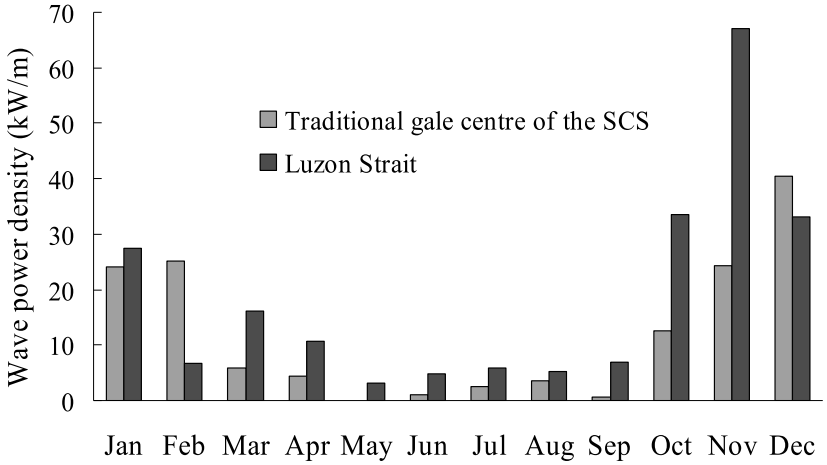

FIGURE 4. Projected values of monthly wave power density in the traditional gale centre of the South China Sea (SCS) and the Luzon Strait in 2019.

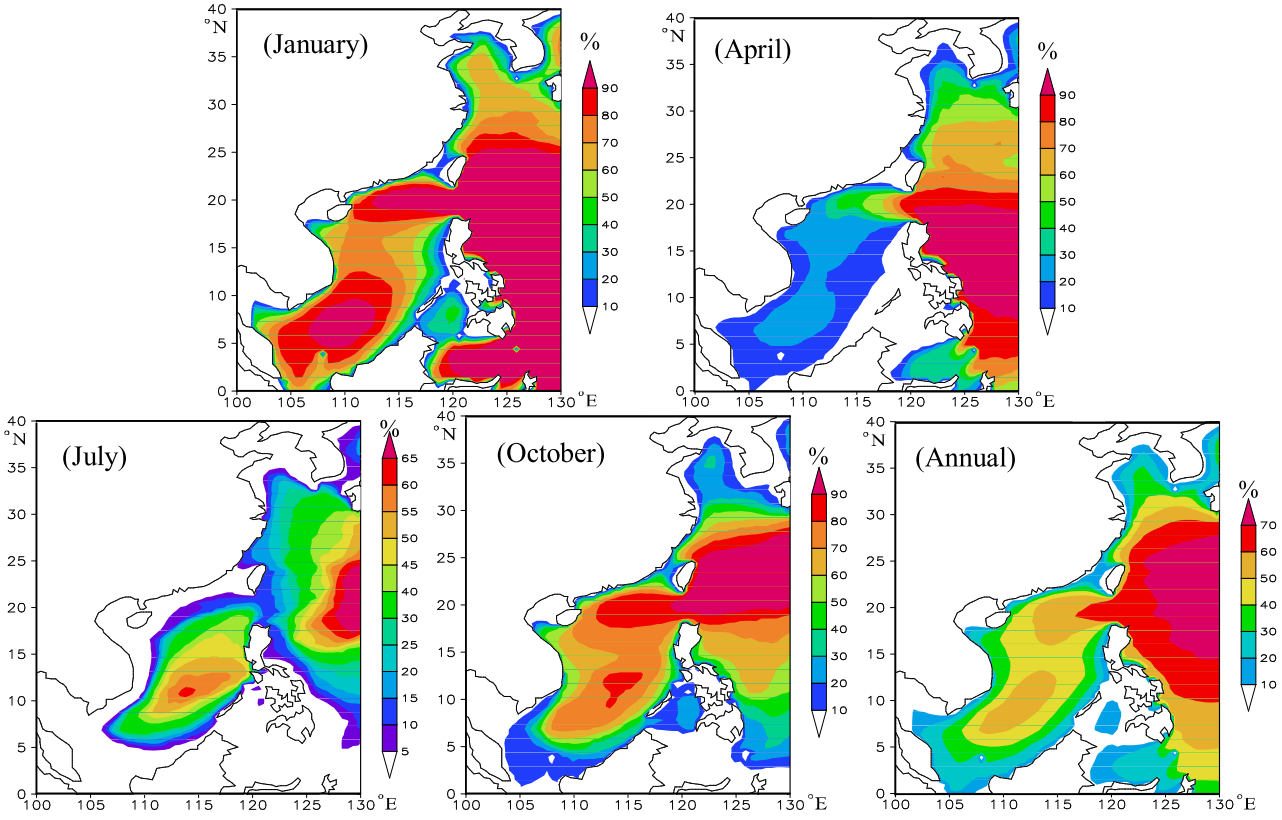

FIGURE 5. Projected occurrence of exploitable significant wave height in the development of wave energy in 2019.

exploitable SWHs in the SCS was much lower than that in January or October, and the occurrence in the ECS was the lowest of the year-round values. In October, the occurrence of exploitable SWHs was lower than that in January but considerably higher than those in April and July. It was >70% in the central-northern areas of the SCS, and most of the central-northern areas of the SCS and most of the south of the ECS had annual occurrences of exploitable SWHs of >40%. A large area of high values was located to the northeast of the Philippines. The occurrence was 10%–40% in the central-southern areas of the middle of the ECS, <40% in the low latitudes of the SCS, and <10% in the north of the ECS, the northern area of the middle of the ECS, the Beibu Gulf, and the Gulf of Thailand.

F. OCCURRENCE OF WPD

To exploit wave energy resources, the occurrence of a WPD greater than a certain energy level is an important

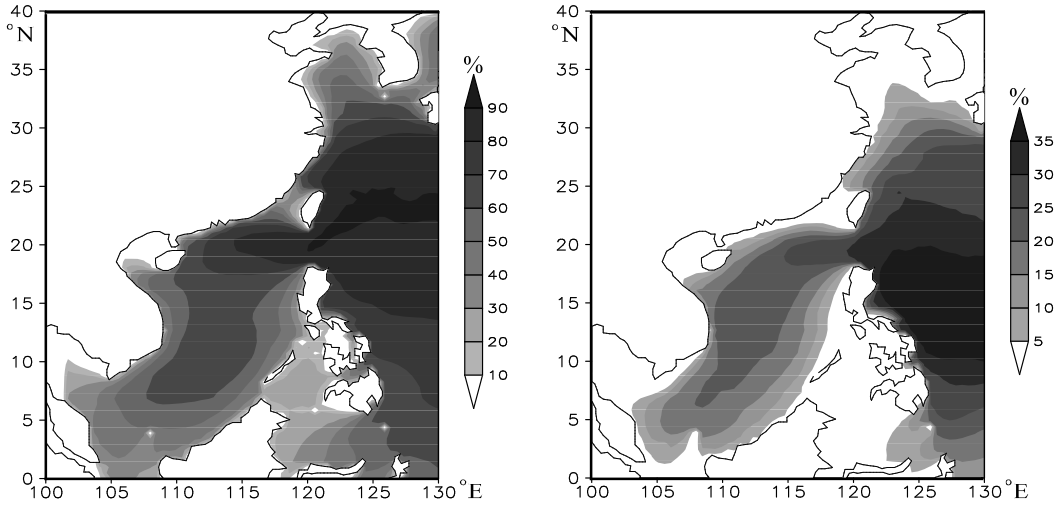

FIGURE 6. Projected values of annual occurrences of wave power density greater than 2 kW/m (left) and greater than 20 kW/m (right) in 2019.

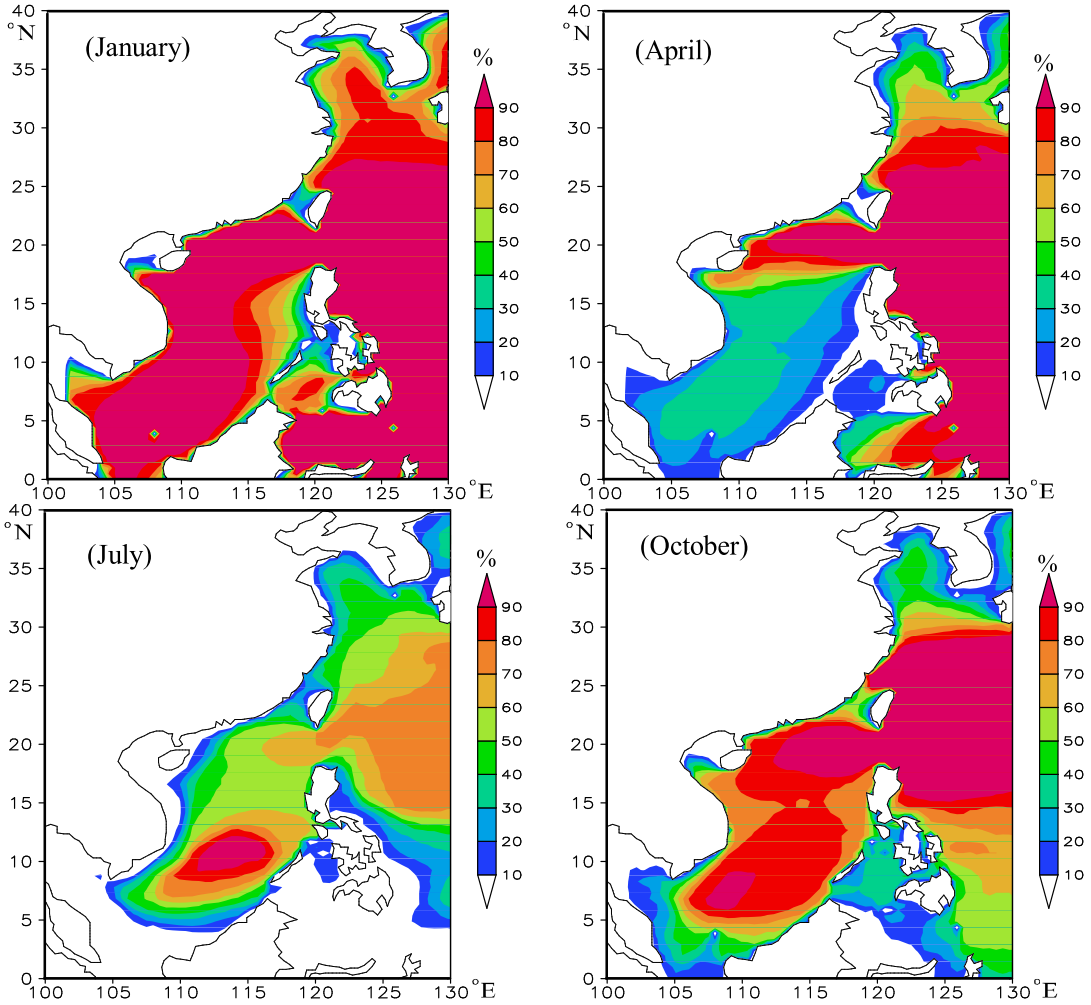

FIGURE 7. Projected values of occurrence of wave power density greater than 2 kW/m in 2019.

factor for quantifying the richness of the wave energy. Usually, wave energy is available when the WPD is >2 kW/m, and areas with WPD > 20 kW/m can be classified as energy-rich regions [38]. This study calculated the percentage of the occurrence of WPD > 2 kW/m and identified the areas where it was >20 kW/m in January, April, July, and October, as well as the annual occurrence (Figures 6–8).

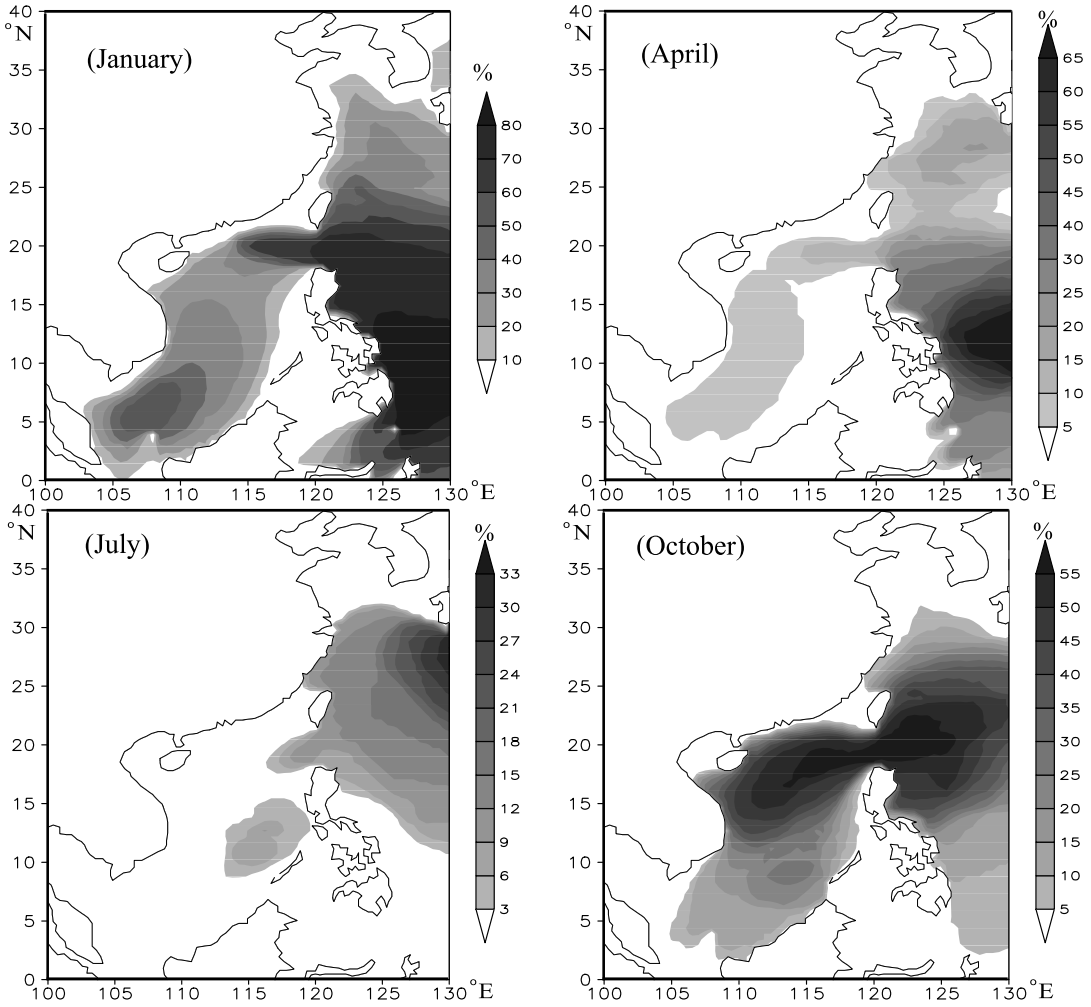

FIGURE 8. Projected values of occurrence of wave power density greater than 20 kW/m in 2019.

1) PROJECTED VALUES FOR THE ANNUAL OCCURRENCE OF WPD >2 kW/m (FIGURE 6a)

The occurrence was >60% in most of the south of the ECS, >40% in most of the SCS, and approximately 30%–60% in the central-southern areas of the middle of the ECS. The low-value areas (<10%) are mainly located in the north of the ECS, the northern area of the middle of the ECS, the Beibu Gulf, and the northern Gulf of Thailand.

2) PROJECTED VALUES FOR THE ANNUAL OCCURRENCE OF WPD > 20 kW/m (FIGURE 6b)

The occurrence was low in the middle and north of the ECS, but the occurrence in most of the SCS is higher at >20%. Another area of relatively high values was located in the eastern waters of the Philippines (>35%).

3) SEASONAL PROJECTED VALUES FOR THE OCCURRENCE OF WPD > 2 kW/m (FIGURE 7)

In January, the occurrence was the highest of the year-round values in almost all of the SCS and the Ryukyu Islands (>90%), and the values were 70%–90% in the south of the ECS and 60%–80% in the central-southern areas of the middle of the ECS. The low-value areas were located in the north of the ECS (<10%), the northern area of the middle of the ECS (<30%), the Taiwan Strait (<30%), the Beibu Gulf (<20%), and the Gulf of Thailand (<30%). In April, the occurrence of WPD > 2 kW/m was lower than that in January and October. The Ryukyu Islands and the Luzon Strait were the high-occurrence areas (>90%), and the occurrence in the traditional gale center of the SCS was 50%–80%. In July, a relatively large area of >70% was distributed in the traditional gale center of the SCS. In October, the occurrence is >60% in most of the SCS and <50% in most of the ECS. A relatively large area of > 90% was distributed in the Luzon Strait and its east waters.

4) SEASONAL PROJECTED VALUES FOR THE OCCURRENCE OF WPD >20 kW/m (FIGURE 8)

In January, the occurrence in most of the SCS is >20%, with relatively high values located in the traditional gale

TABLE 1. Projected annual mean values of the wave energy parameters of the different regions in 2019.

Region	WPD (kW/m)	Occurrence of exploitable SWH (%)	Occurrence of WPD greater than 2 kW/m (%)	Occurrence of WPD greater than 20 kW/m (%)
North of the ECS	<3	<10	<10	<5
Middle of the ECS	<3 along the coast and in the north, 3-6 in the south	<10 along the coast of the northern region, 10-40 in the mid-southern region	<10 along the coast of the northern region, 10-60 in the mid-southern region	<5 in most waters
South of the ECS	6-15	40-70	60-90	<5 along the coast, 5-20 in the offshore regions
South China Sea	6-21 in most waters	10-60 in most waters	40-80 in most waters	5-30 in most waters

center of the SCS (>40%) and the Luzon Strait (>60%). In April and July, the occurrences were much lower than those in January and October. In October, large values (>50%) were noted in the northern SCS and northeastern waters of the Philippines. Judging from the occurrence of WPD > 20 kW/m, the energy-rich regions were mainly located in the northern SCS. The indigent areas were mainly distributed in the north and middle of the ECS, the Beibu Gulf, and the Gulf of Thailand.

G. COMPARISON OF THE PROJECTED WAVE ENERGY AMONG DIFFERENT REGIONS

To compare the projected wave energy parameters among the different regions, this study evaluated four wave energy parameters (the projected annual mean WPDs and the occurrences of exploitable SWH, WPD > 2 kW/m, and WPD > 20 kW/m) in the different regions of the ECS and SCS (Table 1). The north of the ECS and the northern areas of the middle of the ECS exhibited low values for all the wave energy parameters. The energy-rich regions were mainly distributed in the SCS and the south of the ECS, especially in the central-southern areas of the south of the ECS and the central-northern areas of the SCS. In the middle and south of the ECS, the values of the four wave energy parameters gradually increased from north to south.

IV. CONCLUSION

This study proposed a projection system for wave energy resources, and the ECS and SCS were selected as case studies. The following results were obtained.

(1) An area of high multiyear average WPDs was observed in the northern SCS, whereas lower values were noted in the north of the ECS, the northern and coastal areas of the middle of the ECS, the Beibu Gulf, the Gulf of Thailand, and the equatorial waters. The south of the ECS and most of the SCS were relatively rich regions in terms of the WPD. The projected WPD in 2019 was similar to the multiyear average WPD in the north and middle of the ECS, slightly higher than multiyear average WPD in the south of the ECS, and higher than the multiyear average WPD in the SCS and the eastern waters of the Philippines.

(2) The multiyear average WPD in January was the highest of the year-round values, followed by October, and it was the lowest in April. In 2019, the WPDs in January, April, and October were considerably higher than the multiyear mean WPDs for the corresponding months. In July, the projected WPDs in the SCS were smaller than the multiyear averages, while the opposite trend was observed in the south of the ECS.

(3) The EWHO in 2019 in the ECS and SCS was optimistic. The EWHO in January was the highest of the year-round values, followed by October. The lowest EWHOs in the ECS and SCS were found in July and April, respectively. In January, the EWHO was >60% in most of the SCS and the south of the ECS and 30%–60% in the central and southern areas of the middle of the ECS. In April, the EWHO was 10%–30% in a large area of the SCS, 20%–50% in most of the south of the ECS, 10%–50% in the central and southern areas of the middle of the ECS, and greater than 90% in the eastern waters of the Philippines. In July, an area of high values was located in the middle of the SCS. In October, the EWHO was slightly lower than that in January.

(4) The projected annual occurrence of WPD > 2 kW/m was >60% in most of the south of the ECS; >40% in most of the SCS; 30%–60% in the central-southern area of the middle of the ECS; and <10% in the north of the ECS, northern area of the middle of the ECS, Beibu Gulf, and northern Gulf of Thailand. The occurrence of WPD > 2 kW/m in January was the highest of the year-round values, followed by October. The lowest occurrences of WPD > 2 kW/m in the ECS and SCS were found in July and April, respectively.

(5) The projected annual occurrence of WPD > 20 kW/m was low in most of the ECS and was higher in the northern SCS (>20%) and eastern waters of the Philippines (>35%). In January, the occurrence in most of the SCS was >20%. In April and July, the occurrences were considerably lower than those in January and October. In October, large values (>50%) were noted in the northern SCS and northeastern Philippines.

REFERENCES

[1] T. H. Soukissian and A. Papadopoulos, "Effects of different wind data sources in offshore wind power assessment," *Renew. Energy*, vol. 77, pp. 101–114, May 2015.

[2] J. Dai, D. Liu, L. Wen, and X. Long, "Research on power coefficient of wind turbines based on SCADA data," *Renew. Energy*, vol. 86, pp. 206–215, Feb. 2016.
[3] T. Soukissian, D. Denaxa, K. Flora, A. Prospathopoulos, K. Sarantakos, A. Iona, K. Georgantas, and S. Mavrakos, "Marine renewable energy in the Mediterranean Sea: Status and perspectives," *Energies*, vol. 10, no. 10, p. 1512, 2017. doi: 10.3390/en10101512.
[4] L. Rusu, D. Ganea, and E. Mereuta, "A joint evaluation of wave and wind energy resources in the Black Sea based on 20-year hindcast information," *Energy Explor. Exploitation*, vol. 36, no. 2, pp. 335–351, Mar. 2018.
[5] S. Ching-Piao, H. Ching-Her, H. Chien, and C. Hao-Yuan, "Study on the wave climate variation to the renewable wave energy assessment," *Renew. Energy*, vol. 38, no. 1, pp. 50–61, Feb. 2012.
[6] G. Xydis, "A wind energy integration analysis using wind resource assessment as a decision tool for promoting sustainable energy utilization in agriculture," *J. Cleaner Prod.*, vol. 96, pp. 476–485, Dec. 2015.
[7] G. Xydis and L. Mihet-Popa, "Wind energy integration via residential appliances," *Energy Efficiency*, vol. 10, no. 2, pp. 319–329, Jun. 2016.
[8] H. Behzad and R. Panahi, "Optimization of bottom-hinged flap-type wave energy converter for a specific wave rose," *J. Mar. Sci. Appl.*, vol. 16, no. 2, pp. 159–165, Apr. 2017.
[9] S. Langodan, Y. Viswanadhapalli, H. P. Dasari, O. Knio, and I. Hoteit, "A high-resolution assessment of wind and wave energy potentials in the Red Sea," *Appl. Energy*, vol. 181, pp. 244–255, Nov. 2016.
[10] L. Rusu and F. Onea, "The performance of some state-of-the-art wave energy converters in locations with the worldwide highest wave power," *Renew. Sustain. Energy Rev.*, vol. 75, pp. 1348–1362, Aug. 2017.
[11] K. Hulls, "Wave power," *New Zealand Energy J.*, vol. 4, pp. 44–48, Apr. 1977.
[12] M. Denis, "Wave climate and the wave power resource," in *Hydrodynamics of Ocean Wave-Energy Utilization*. Berlin, Germany: Springer, 1986, pp. 133–156.
[13] A. M. Cornett, "A global wave energy resource assessment," in *Proc. 18th Int. Offshore Polar Eng. Conf.*, Vancouver, BC, Canada, Jan. 2008, pp. 6–11.
[14] B. Aydogan, B. Ayat, and Y. Yuksel, "Black Sea wave energy atlas from 13 years hindcasted wave data," *Renew. Energy*, vol. 57, pp. 436–447, Sep. 2013.
[15] C. W. Zheng and C. Y. Li, "An overview and suggestions on the difficulty of site selection for marine new energy power plant—Wave energy as a case study," *J. Harbin Eng. Univ.*, vol. 39, no. 2, pp. 200–206, Feb. 2018.
[16] J. P. Sierra, M. Casas-Prat, and E. Campins, "Impact of climate change on wave energy resource: The case of Menorca (Spain)," *Renew. Energy*, vol. 101, pp. 275–285, Feb. 2017.
[17] R. Atlas, R. N. Hoffman, J. Ardizzone, S. M. Leidner, J. C. Jusem, D. K. Smith, and D. Gombos, "A cross-calibrated, multiplatform ocean surface wind velocity product for meteorological and oceanographic applications," *Bull. Amer. Meteorol. Soc.*, vol. 92, no. 2, pp. 157–174, Dec. 2011.
[18] K. E. Taylor, R. J. Stouffer, and G. A. Meehl, "An overview of CMIP5 and the experiment design," *Bull. Amer. Meteorol. Soc.*, vol. 93, no. 4, pp. 485–498, 2012.
[19] B. Kirtman, S. B. Power, J. A. Adedoyin, G. J. Boer, R. Bojariu, I. Camilloni, F. J. Doblas-Reyes, A. M. Fiore, M. Kimoto, G. A. Meehl, M. Prather, A. Sarr, C. Schã, R. Sutton, G. J. van Oldenborgh, G.Vecchi, and H. J. Wang, "Near-term climate change: Projections and predictability," in *The Physical Science Basis. Contribution of Working Group I to the Fifth Assessment Report of the Intergovernmental Panel on Climate Change*. Cambridge, U.K.: Cambridge, Univ. Press, 2013.
[20] M. Collins, M. R. Knutti, J. Arblaster, J. L. Dufresne, T. Fichefet, P. Friedlingstein, X. Gao, W. J. Gutowski, T. Johns, G. Krinner, M. Shongwe, C. Tebaldi, A. J. Weaver, and M. Wehner, "Long-term climate change: Projections, commitments and irreversibility," in *The Physical Science Basis. Contribution of Working Group I to the Fifth Assessment Report of the Intergovernmental Panel on Climate Change*. Cambridge, U.K.: Cambridge, Univ. Press, 2013.
[21] X. L. Wang, Y. Feng, and V. R. Swail, "Changes in global ocean wave heights as projected using multimodel CMIP5 simulations," *Geophys. Res. Lett.*, vol. 41, no. 3, pp. 1026–1034, Feb. 2014.
[22] N. Mori, T. Yasuda, H. Mase, T. Tom, and Y. Oku, "Projection of extreme wave climate change under global warming," *Hydrol. Res. Lett.*, vol. 4, pp. 15–19, Jan. 2010.
[23] P. C. Chu, Y. Q. Qi, Y. C. Chen, P. Shi, and Q. W. Mao, "South China Sea wind-wave characteristics. Part I: Validation of wavewatch-III using TOPEX/Poseidon data," *J. Atmos. Ocean. Technol.*, vol. 21, no. 11, pp. 1718–1733, Nov. 2004.
[24] B. Liang, H. Li, and D. Lee, "Numerical study of three-dimensional suspended sediment transport in waves and currents," *Ocean Eng.*, vol. 34, nos. 11–12, pp. 1569–1583, Aug. 2007.
[25] B. C. Liang, X. Liu, H. Li, Y. Wu, and D. Lee, "Wave climate hindcasts for the Bohai Sea, Yellow Sea, and East China Sea," *J. Coastal Res.*, vol. 32, no. 1, pp. 172–180, Jan. 2016.
[26] A. Mirzaei, F. Tangang, L. Juneng, M. A. Mustapha, M. L. Husain, and M. F. Akhir , "Wave climate simulation for southern region of the South China Sea," *Ocean Dyn.*, vol. 63, no. 8, pp. 961–977, Aug. 2013.
[27] M. Dobrynin, J. Murawsky, and S. Yang, "Evolution of the global wind wave climate in CMIP5 experiments," *Geophys. Res. Lett.*, vol. 39, no. 18, Sep. 2013, Art. no. L18606. doi: 10.1029/2012GL052843.
[28] M. A. Hemer and C. E. Trenham, "Evaluation of a CMIP5 derived dynamical global wind wave climate model ensemble," *Ocean Model.*, vol. 103, pp. 190–203, Jul. 2016.
[29] M. Casas-Prat, X. L. Wang, and N. Swart, "CMIP5-based global wave climate projections including the entire Arctic Ocean," *Ocean Model.*, vol. 123, pp. 66–85, Mar. 2018.
[30] C. Zheng, R. Zhang, W. Shi, X. Li, and X. Chen, "Trends in significant wave height and surface wind speed in the China Seas between 1988 and 2011," *J. Ocean Univ. China*, vol. 16, no. 5, pp. 717–726, May 2017.
[31] G. Iglesias and R. Carballo, "Choosing the site for the first wave farm in a region: A case study in the Galician Southwest (Spain)," *Energy*, vol. 36, no. 9, pp. 5525–5531, Sep. 2011.
[32] A. Vosough, "Wave power," *Int. J. Multidisciplinary Sci. Eng.*, vol. 2, no. 7, pp. 60–63, Jul. 2011.
[33] Y. Wan, J. Zhang, J. Meng, and J. Wang, "Exploitable wave energy assessment based on ERA-Interim reanalysis data—A case study in the East China Sea and the South China Sea," *Acta Oceanol. Sinica*, vol. 34, no. 9, pp. 143–155, Sep. 2015.
[34] Y. Wan, J. Zhang, J. Meng, J. Wang, and Y. Dai, "Study on wave energy resource assessing method based on altimeter data—A case study in Northwest Pacific," *Acta Oceanol. Sinica*, vol. 35, no. 3, pp. 117–129, Mar. 2016.
[35] N. Mori, M. A. Hemer, P. Lionello, and F. J. Mendez, "Projections of future wave cimate for marine renewable energy," in *Proc. Grand Renew. Energy*, Tokyo Big Sight, Tokyo, Jpn., 2016, pp. 1–5.
[36] M. A. Hemer, Y. Fan, N. Mori, A. Semedo, and X. L. Wang, "Projected changes in wave climate from a multi-model ensemble," *Nature Climate Change*, vol. 3, pp. 471–476, Jan. 2013.
[37] P. Camus, I. J. Losada, C. Izaguirre, A. Espejo, M. Menéndez, and J. Pérez, "Statistical wave climate projections for coastal impact assessments," *Earth's Future*, vol. 5, no. 9, pp. 918–933, Sep. 2017.
[38] J. L. Ren, Y.-Y. Luo, and J.-J. Chen, X.-M. Zhang, and Y.-J. Zhong, "Research on wave power application by the information system for ocean wave resources evaluation," *Renew. Energy Resour.*, vol. 27, no. 3, pp. 93–97, Jan. 2009.

CHONG-WEI ZHENG received the Ph.D. degree in atmospheric sciences from the National University of Defense Technology. He is currently a Guest Professor with Ludong University, a Visiting Research Fellow with the College of Marine Science, Sun Yat-sen University, and a Senior Visiting Scholar with the State Key Laboratory of Estuarine and Coastal Research. He has published more than 90 papers in many peer-reviewed journals as the first author or corresponding author, including 24 papers indexed by Science Citation Index (SCI) and 12 papers in journals included in the Ei Compendex. He has published six books as the first author. His main research interests include marine new energy evaluation and physical oceanography. He is a Reviewer for more than 40 high-impact journals, including *Applied Energy*, *Remote Sensing of the Environment*, *Journal of Environmental Management*, *Clean Technologies and Environmental Policy*, *Ocean Science*, and *Deep-Sea Research Part I*. He is also a Monograph Reviewer for the Elsevier.

GUO-XIANG WU received the Ph.D. degree in coastal engineering from the Ocean University of China (OUC), where he is currently an Associate Professor with the College of Engineering. He has published 15 SCI-indexed journal papers as the first author or coauthor. His main research interests include hydrodynamics and sediment transport in coastal systems, such as estuaries, river deltas, and salt marshes.

XUAN CHEN received the master's degree in physical oceanography from the College of Meteorology and Oceanography, PLA University of Science and Technology. He is an Engineer with The 75839 Army of the PLA. Recently, he and his collaborators presented a more generalized linear regression model that can be used to analyze the relationship between two fields, gave a new explanation of Pacific equatorial undercurrent, proposed a reduction-order algorithm for 3DVAR within the Sylvester equation, and, accordingly, gave a Typhoon activity frequency monitoring index in the Typhoon active period. His research interests include physical oceanography, and statistic and numerical simulation.

QING WANG received the Ph.D. degree from Peking University, in 1997, and the Postdoctoral Research work from the State Key Laboratory of Estuarine and Coastal Research, from 1997 to 1999. He is currently a Professor with Ludong University. His research interest includes coastal ocean dynamics.

ZHAN-SHENG GAO is currently a Professor with the Dalian Naval Academy. His main research interest includes navigation and ocean environment analysis. He has published more than ten papers in many peer-reviewed journals. He has authored four books and book chapters.

YUN-GE CHEN received the M.S. degree in chemistry from the North University of China. She is currently an Assistant Engineer with the Dalian Naval Academy. Her main research interest includes ocean environment analysis.

XIA LI received the Ph.D. degree from the National University of Defense Technology. She was a Research Scholar with the Center for Anal-ysis and Prediction of Storms (CAPS), The Uni-versity of Oklahoma. She is currently a Lecturer with the College of Meteorology and Oceanology, National University of Defense Technology. Her research interests include the severe convective systems in the aspects of their convection initia-tions, development mechanisms, ensemble predictions, and the sea–air interactions, mainly regarding the interactions between the tropical cyclones and the sea.